Electromagnetic response in strong magnetic fields. II. Particle polarization and mode structure for parallel propagation

R. A. Cover
R and D Associates, P. O. Box 9695, Marina del Rey, California 90291

G. Kalman
Department of Physics, Boston College, Chestnut Hill, Massachusetts 02167

P. Bakshi
Department of Physics, Boston College, Chestnut Hill, Massachusetts 02167

(Received 23 April 1979)

The particle part of the polarization matrix for a relativistically dense electron gas in an external magnetic field is explicitly calculated for the case of propagation vector $\vec{k}$ parallel to the magnetic field. The results are combined with the corresponding renormalized vacuum elements to give the complete ω- and k-dependent dielectric response function $\epsilon_{ij}(\vec{k},\omega)$ for the system. The static longitudinal element $\epsilon_{\parallel}(\vec{k},0)$ is used to determine the density and field dependence of the screening along the field. The static transverse element $\epsilon_{\perp}(\vec{k},0)$ determines the magnetic properties of the system. The possibility of magnetic phase transitions is determined for densities greater than a certain B-dependent value. The longitudinal $k = 0$ element $\epsilon_{\parallel}(0,\omega)$ is used to investigate the longitudinal plasma mode and the associated plasma frequency of the system; its remarkable magnetic field dependence is displayed. The Landau-level structure of the plasma and the vacuum contribution have important effects on the structure of the mode. The transverse $k = 0$ left-handed $\epsilon_{+}(0,\omega)$ and right-handed $\epsilon_{-}(0,\omega)$ elements are employed to analyze the transverse modes and to investigate ω_{φ}, the associated cyclotron resonance. The latter acquires a complex fine structure owing to the relativistic Landau energy states of the system.

I. INTRODUCTION

The collective properties of a many-body system, such as the ground-state energy, magnetic properties, and structure and propagation of collective modes, can be determined from the dielectric tensor of the system. The properties of a relativistic quantum plasma in an external magnetic field, apart from their intrinsic theoretical interest, are relevant to models of collapsed stars. The questions one is concerned with relate to the equilibrium properties, to the electric and magnetic response characteristics of the system, and finally to the structure and propagation of collective modes. A central object for the study of all these features is the polarization matrix or, equivalently, the dielectric response function.

The properties of a relativistically dense electron gas in a neutralizing background in an external magnetic field have not received any substantial treatment in the literature. The modern literature on the properties of a nonrelativistic quantum electron gas in intense magnetic fields, however, extends back to the early 1960's. Stephen[1] used Green's-function techniques to calculate the longitudinal dispersion relation for propagation vector parallel and perpendicular to the magnetic field. This problem was analyzed in more detail by Horing,[2] particularly with respect to perpendicular propagation and the damping associated with the modes. In subsequent articles Horing considered in detail the longitudinal static limit and the effective dielectric screening along and transverse to the field.[3] The elements of the dielectric tensor for spinless electrons were calculated by Quinn and Rodriquez.[4] The static limit of these elements was used by Quinn[5] to calculate the diamagnetic susceptibility of this system. The complete dielectric tensor, including the effect of collisions, for this system, in the case of parallel and perpendicular propagation, was given by Green *et al.*[6] The work by Green *et al.* contains additional discussion of and references to work on diamagnetic interactions. Subsequently, Chiu and Canuto studied the equation of state and thermodynamic properties of an electron gas by evaluating the energy-momentum tensor using the exact wave-function solutions of the Dirac or Schrödinger equation.[7] Canuto and Ventura included the effect of spin in calculating the nonrelativistic dielectric tensor.[8] Magnetic instabilities and phase transitions were derived and examined by Quinn[9] and by Lee *et al.*[10]

At the other end of the spectrum the *relativistic* electron gas, without an external magnetic field, was described by Tsytovitch[11] (also see Kalman and Prasad[12]).

The above studies already made it clear that, for a relativistic system, it was not feasible to

 © 1979 The American Physical Society

divorce the calculation of the vacuum contribution to the polarization matrix from that of its particle contribution. Thus, the investigation of a relativistic quantum plasma in a magnetic field requires a unified formalism for the calculation of the corresponding combined vacuum and particle polarization matrix. Such a formalism we developed in a previous paper[13] (I). This previous work constitutes the framework of the present paper, whose aim is to study the properties of the many-body system we have described. The important qualitative features result mostly and not surprisingly from the particle contribution. These features, in the case that pertains to static properties, appear as straightforward generalizations of the quantum, nonrelativistic limit. The collective modes, however, are significantly modified by the relativistic effects.

The principal restriction both in I and in the present work is that we only calculate the case where the propagation vector $\vec{k}$ is parallel to the external magnetic field $\vec{B}$. We ignore all temperature effects, considering only the $T=0$ case. We do not impose any restriction on the value of the magnetic field, but our main interest lies in analyzing the behavior of the system for very strong ($B \geq B_* \equiv 4.4\times 10^{13}$ G) magnetic fields; this also implies that in most cases we will be concerned with systems populating the few lowest-lying Landau levels only. A further simplification that we will use at a later point is that, although we evaluate the full $\vec{k}$- and ω-dependent polarization matrix, $\vec{\Pi}(\vec{k},\omega)$ and dielectric tensor $\vec{\epsilon}(\vec{k},\omega)$, we investigate the $\vec{\epsilon}(\vec{k},0)$ and $\vec{\epsilon}(\vec{0},\omega)$ limits only: This simplification will be commented upon later in the text.

After reviewing the general formalism in the present section, in Sec. II we study the static longitudinal (electric) polarizability and the associated screening length. In Sec. III the corresponding transverse magnetic polarizability and the possible magnetic phase transition are analyzed. Section IV describes the longitudinal collective modes, plasma oscillation and the recently discovered "longitudinal photon" mode, and the unusual density and magnetic field dependence of the plasma frequency. Section V describes the ordinary and extraordinary transverse modes and in particular the important modification of the cyclotron-resonance structure.

A. Review of general formalism

We will outline the formalism developed in I for the calculation of the particle and vacuum polarization matrix. The dielectric function $\vec{\epsilon}(\vec{k},\omega)$ and the differential diamagnetic function $\vec{\nu}(\vec{k},\omega)$ of a many-body system relate differentially small applied field $\hat{E}_i$ and $\hat{B}_i$ to the physical fields E_i and B_i and electric polarization $\vec{P}$ and magnetization $\vec{M}$ by

$$E_i=(\epsilon^{-1})_{ij}\hat{E}_j\,,\qquad B_i=(\nu^{-1})_{ij}\hat{B}_j\,. \tag{1}$$

These response functions can be expressed in terms of electric and differential magnetic polarizabilities $\vec{\alpha}(\vec{k},\omega)$ and $\vec{\xi}(\vec{k},\omega)$ ($\hbar=c=1$):

$$\vec{P}=\vec{\alpha}\vec{E}\,,\quad \vec{D}=\vec{E}+\vec{P}\,,\qquad \vec{M}=-\vec{\xi}\vec{B}\,,\quad \vec{H}=\vec{B}-\vec{M}\,, \tag{2a}$$

from which it follows that

$$\vec{\epsilon}=\vec{1}-\omega^2\vec{\Delta}^{-1}\vec{\alpha}\,,\qquad \vec{\nu}=\vec{1}+k^2\vec{\Delta}^{-1}\vec{\xi}\,,\qquad \vec{\Delta}=(k^2-\omega^2)\vec{1}-\vec{k}\vec{k}\,, \tag{2b}$$

which in turn are related to the spacelike part of the polarization matrix via

$$\alpha_{ij}(\vec{k},\omega,B)=-\frac{1}{\omega^2}\,\bar{\Pi}_{ij}(\vec{k},\omega,B)\,,\qquad \xi_{ij}(\vec{k},\omega,B)=-\frac{1}{k^4}\,k_m\epsilon_{imp}\bar{\Pi}_{pq}(\vec{k},\omega,B)\epsilon_{jqn}k_n\,, \tag{3}$$

where $\bar{\Pi}_{\mu\nu}$ is the fully regularized polarization matrix. Note that while our definitions of $\vec{\alpha}$ and $\vec{\xi}$ are in accord with convention, $\vec{\epsilon}$ and $\vec{\nu}$ are somewhat different and have been chosen so that the relations expressed by Eq. (1) remain valid for arbitrary polarization of $\vec{E}$ and $\vec{B}$. This is not the case for the conventional definition, where $\vec{\epsilon}=\vec{1}+\vec{\alpha}$ and $\vec{\nu}=\vec{1}+\vec{\xi}$.

Using the formalism given in I, one can write down the polarization matrix for a system consisting of a relativistic positron and electron gas with distribution functions $n^{\pm}(\epsilon_{ps})$, respectively. The polarization matrix comprises three pieces: $\Pi^{\pm}_{\mu\nu}(\vec{k},\omega)$ pertaining to the positrons and electrons, and $\Pi^{0}_{\mu\nu}(\vec{k},\omega)$ pertaining to the vacuum. The results given in I were calculated to lowest order e^2. In the language of many-body theory, this corresponds to the conventional random-phase approximation (RPA):

$$\Pi^{-}_{\mu\nu}(\vec{k},\omega)=-\frac{e^3B}{2\pi}\sum_{s,\bar{s}}\int dp\,\frac{1}{2\epsilon_{ps}\epsilon_{\bar{p}\bar{s}}}\left\{\frac{R_{\mu\nu}(\vec{k})}{\omega-(\epsilon_{\bar{p}\bar{s}}-\epsilon_{ps})}\left[n^{-}(\epsilon_{\bar{p}\bar{s}})-n^{-}(\epsilon_{ps})\right]-\frac{P_{\mu\nu}(\vec{k})}{\omega-(\epsilon_{\bar{p}\bar{s}}+\epsilon_{ps})}\,n^{-}(\epsilon_{\bar{p}\bar{s}})+\frac{P_{\mu\nu}(\vec{k})}{\omega+(\epsilon_{\bar{p}\bar{s}}+\epsilon_{ps})}\,n^{-}(\epsilon_{ps})\right\}, \tag{4}$$

$$\Pi^{0}_{\mu\nu}(\vec{k},\omega)=-\frac{e^3B}{2\pi}\sum_{s,\bar{s}}\int dp\,\frac{\epsilon_{ps}+\epsilon_{\bar{p}\bar{s}}}{\epsilon_{ps}\epsilon_{\bar{p}\bar{s}}}\,\frac{P_{\mu\nu}(\vec{k})}{\omega^2-(\epsilon_{\bar{p}\bar{s}}+\epsilon_{ps})^2}\,, \tag{5}$$

$$P_{\mu\nu}(\vec{k}) \equiv \int \mathrm{tr}\gamma_\mu \overline{\Lambda}(\vec{p}, -\epsilon_{\bar{p}\bar{s}}) D_{\bar{s}}(r) \gamma_\nu \overline{\Lambda}(p, \epsilon_{ps}) D_s(r) e^{i\vec{k}\cdot\vec{r}} d\vec{r}\,, \tag{6}$$

where

$$p = p_3$$

and

$$\begin{aligned} \bar{p} &= p + k\,, \\ \epsilon_{ps} &= (p^2 + m^2 + 2seB)^{1/2} \end{aligned} \tag{7}$$

is the single-particle energy. The general form of the elements $R_{\mu\nu}(\vec{k})$ and $P_{\mu\nu}(\vec{k})$ is given in I. In this work we will only consider the case $\vec{k} = k\hat{z}$, i.e., $\vec{k}$ parallel to $\vec{B}$ $(=B\hat{z})$. In this case, the $P_{\mu\nu}$'s reduce to

$$\begin{aligned} P_{11} &= -2(p\bar{p} + m^2 + \epsilon_{ps}\epsilon_{\bar{p}\bar{s}}) \\ &\quad \times (\delta_{s,\bar{s}-1} + \delta_{s,\bar{s}+1}) \\ &= P_{22}\,, \\ P_{33} &= -2(-p\bar{p} + m^2 + 2seB + \epsilon_{ps}\epsilon_{\bar{p}\bar{s}}) \\ &\quad \times (\delta_{s,\bar{s}} + \delta_{s-1,\bar{s}-1})\,, \\ P_{21} &= -2i(p\bar{p} + m^2 + \epsilon_{ps}\epsilon_{\bar{p}\bar{s}}) \\ &\quad \times (\delta_{s,\bar{s}+1} - \delta_{s,\bar{s}-1}) \\ &= -P_{12}\,, \\ P_{23} &= P_{32} = P_{13} = P_{31} = 0\,, \end{aligned} \tag{8}$$

with $R_{\mu\nu}(k)$ obtained from $P_{\mu\nu}(k)$ by a $-\epsilon_{\bar{p}\bar{s}} \rightleftarrows \epsilon_{\bar{p}\bar{s}}$ replacement. Our interest is in ultradense systems where the Fermi energy is very high and temperature effects negligible. Thus we have assumed that $n^-(\epsilon) = \theta(\epsilon_F - \epsilon)$ and $n^+(\epsilon) = 0$.

B. Degenerate Fermi gas in an external magnetic field

To establish the energy and momentum relationships used in the remainder of the paper, we will review the description of a noninteracting relativistically degenerate electron gas in an external magnetic field.

The quantized total energy of a free relativistic electron in a uniform external magnetic field is

$$\epsilon_{ps} = (p^2 + m^2 + 2seB)^{1/2}\,, \tag{9}$$

where p is the momentum along the field, and $s = 0, 1, 2, \ldots$ is the quantum number characterizing the Landau level of the electron. The multiplicity of each Landau level due to the coalescing of the free transverse-momentum states into those of a two-dimensional harmonic oscillator[14] is

$$\begin{aligned} D &= \frac{V^{2/3}}{(2\pi\hbar)^2} \int_0^{2\pi} d\phi \int_{2se\hbar B/c}^{2(s+1)e\hbar B/c} \tfrac{1}{2} dp_\perp^{\,2} \\ &= V^{2/3} \frac{eB}{2\pi\hbar c}\,, \end{aligned} \tag{10}$$

where $\hbar$ and c have been given explicitly. In addition, there is a level degeneracy due to spin:

$$\begin{aligned} a_s &= 1 \text{ for } s = 0\,, \\ a_s &= 2 \text{ for } s > 0\,. \end{aligned} \tag{11}$$

The electrons then occupy levels $s = 0, 1, \ldots$ up to some Fermi level s_F, which may be partially or completely filled. The word "filled" is used in a special sense. A given level s will be referred to as filled if the fermion number density is such that the $(s+1)$ level is occupied or, in the case of the s_F level, if an addition to the density causes the $(s_F + 1)$ level to be entered. The Fermi energy of the system is given by

$$\epsilon_F = (p_s^{\,2} + m^2 + 2seB)^{1/2}\,, \tag{12}$$

where p_s is the longitudinal Fermi momentum necessary to take the electron from the sth level to the top of the Fermi sea. The relation between the various p_s's is

$$p_{s-1} = (p_s^{\,2} + 2eB)^{1/2}\,. \tag{13}$$

This gives s_F relations between the $(s_F + 1)$ p_s's. The magnitude of p for a given s is restricted by $0 \le p \le p_s$. To determine the p_s's and the resulting Fermi energy we relate the density of the electrons to the sum over states:

$$\begin{aligned} n &= \frac{eB}{2\pi} \sum_{s=0}^{s_F} a_s \int_{-p_s}^{p_s} dp/2\pi \\ &= \frac{eB}{2\pi^2} \sum_{s=0}^{s_F} a_s p_s\,. \end{aligned} \tag{14}$$

These $(s_F + 1)$ relations allow us to determine the p_s's and thus the resulting Fermi energy. A simple limit results if the top level is completely filled, in which case

$$p_{s_F}^* = (2eB)^{1/2}\,. \tag{15}$$

Graphs of ϵ_F and p_s vs B for a given density are given in Figs. 1 and 2. Note that neither ϵ_F nor p_s is a continuously differentiable function (even though the total energy is).

II. STATIC LONGITUDINAL POLARIZATION AND SCREENING LENGTH

The total polarizability includes the vacuum contribution calculated in detail in I and the electron contribution $\tilde{\Pi}^-(k, \omega)$, which is the main concern of the present work. We will simplify notation by using $\tilde{\Pi}$ in place of $\tilde{\Pi}^-$, and by referring to the total $\tilde{\Pi}$ and $\tilde{\alpha}$ as $\tilde{\Pi}^T$ and $\tilde{\alpha}^T$ when necessary. We

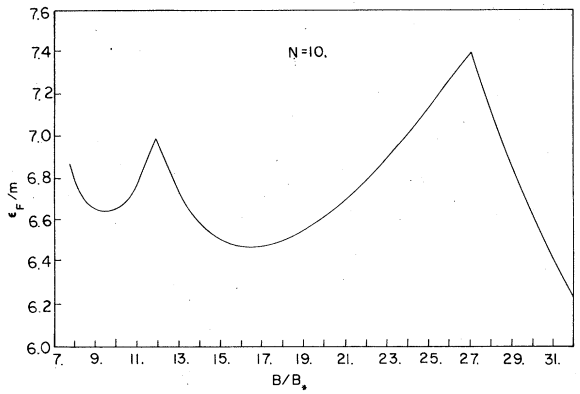

FIG. 1. ϵ_F in units of electron mass m versus B in units of $B_* \equiv m^2/e = 4.4\times10^{13}$ G. The density is measured in units of (Compton wavelength)$^{-3}$. A density of $n=1$ is equivalent to $1.74\times10^{31}/\mathrm{cm}^3 \equiv N_c$. Here $n=10N_c$.

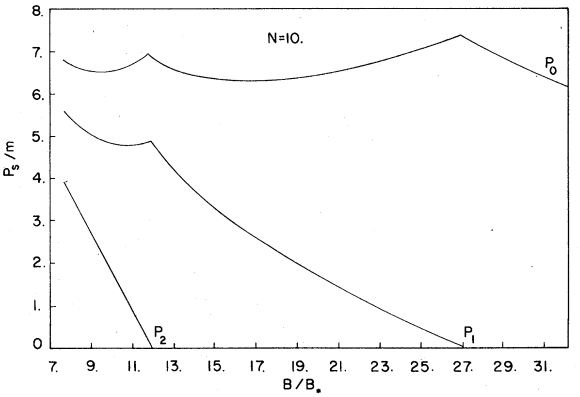

FIG. 2. p_s versus B for $n=10N_c$.

consider first the static limit of the longitudinal polarization $\Pi_{33}(k,0)$. Since the ordinary static susceptibility

$$\alpha_{33}(k,0) = -\lim_{\omega\to0}\Pi_{33}(k,\omega)/\omega^2 \tag{16}$$

should remain finite as ω goes to zero, we expect

$$\Pi_{33}(k,0)=0\,,\qquad -\frac{\partial\Pi_{33}(k,\omega)}{\partial\omega^2}\bigg|_{\omega=0} = \alpha_{33}(k,0)\,. \tag{17}$$

Now, from Eq. (4),

$$\Pi_{33}(k,0) = -\frac{e^3B}{2\pi}\sum_{s,s}\int dp\left\{\frac{[n(\epsilon_{ps})-n(\epsilon_{\bar p\bar s})]R_{33}(k)}{2\epsilon_{ps}\epsilon_{\bar p\bar s}(\epsilon_{\bar p\bar s}-\epsilon_{ps})} + \frac{n(\epsilon_{ps})P_{33}(k)}{\epsilon_{\bar p\bar s}\epsilon_{ps}(\epsilon_{ps}+\epsilon_{\bar p\bar s})}\right\}. \tag{18}$$

After some algebra this yields

$$\Pi_{33}(k,0) = 4\frac{e^3B}{2\pi}\sum_{n=0}^{n_s} a_s\int_{-p_s}^{p_s}\frac{-p}{k\epsilon_{ps}} = 0\,. \tag{19}$$

Expanding $\Pi_{33}(k,\omega)$ in a series in ω^2, we get

$$\begin{aligned}\alpha_{33}(k,0) &\equiv -\frac{\partial\Pi_{33}(k,\omega)}{\partial\omega^2}\bigg|_{\omega=0}\\ &= -\frac{e^3B}{2\pi}\sum_{s,\bar s}\int_{-\infty}^{\infty}dp\left\{\frac{[n(\epsilon_{\bar p\bar s})-n(\epsilon_{ps})]R_{33}(k)}{2\epsilon_{ps}\epsilon_{\bar p\bar s}(\epsilon_{ps}-\epsilon_{\bar p\bar s})} + \frac{n(\epsilon_{ps})P_{33}(k)}{\epsilon_{ps}\epsilon_{\bar p\bar s}(\epsilon_{\bar p\bar s}+\epsilon_{ps})^3}\right\}\\ &= +4\frac{e^3B}{2\pi}\sum_{s=0}^{s_F} a_s\int_{-p_s}^{p_s}\frac{dp}{k^3}\left[\frac{p}{\epsilon_{ps}}+\frac{2(m^2+2seB)}{\epsilon_{ps}(2p+k)}\right]\\ &= -4\frac{e^3B}{2\pi}\sum_{s=0}^{s_F} a_s\frac{m^2+2seB}{(m^2+2seB+k^2/4)^{1/2}}\frac{1}{k^3}\cdot\\ &\qquad\times\ln\left|\frac{-(k/2)p_s+m^2+2seB+\epsilon_F(m^2+2seB+k^2/4)^{1/2}}{(k/2)p_s+m^2+2seB+\epsilon_F(m^2+2seB+k^2/4)^{1/2}}\,\frac{-p_s+k/2}{p_s+k/2}\right|.\end{aligned} \tag{20}$$

In the nonrelativistic limit, this reduces to

$$\alpha_{33}^{\mathrm{NR}}(k,0) = -4\frac{e^3B}{2\pi}\frac{m}{k^3}\sum_{s=0}^{s_F} a_s\ln\left|\frac{p_s-k/2}{p_s+k/2}\right|, \tag{21}$$

which formally agrees with the calculation of Quinn and Rodriquez.

As k goes to 0, Eq. (20) reduces to

$$\alpha_{33}(k,0) = +4\frac{e^3B}{2\pi}\frac{1}{k^2}\sum_{s}^{s_F} a_s(m^2+2seB)^{1/2}\left\{\frac{1}{p_s}+\frac{p_s}{(m^2+2seB)^{1/2}[\epsilon_F+(m^2+2seB)]^{1/2}}\right\}\equiv\frac{\kappa^2}{k^2}\,. \tag{22}$$

We see that the relativistic expression has the same decaying oscillatory long-wavelength behavior that is exhibited by the nonrelativistic limit. That is, as k goes to zero, $\alpha_{33}(k,0)$ goes as $1/k^2$, and the oscillatory behavior is manifested in the (s_F+1) singularities at $k=2p_s$. As k goes to infinity, the polarizability approaches zero as $1/k^4$. This behavior is the same as that without a magnetic field. The large-k behavior of the total polarizability is determined by the vacuum contribution which goes as $-\ln k$. A graph of the static polarizability is given in Fig. 3.

The effective charge of a test particle in the plasma medium is the bare charge modified by the plasma dielectric properties. The imaginary value of k for which the longitudinal dielectric function vanishes determines the longitudinal screening length of the plasma. That is, we seek a solution to the equation

$$1+\alpha_{33}^{T}(k,0)=0\,. \tag{23}$$

For small k the screening length is given by the square root of the factor multiplying $1/k^2$ in the small-k limit, Eq. (22). In this limit the vacuum contribution goes as a constant α_0 plus a term proportional to k^2. The dispersion relation is then modified by vacuum effects to

$$1+\kappa^2/k^2+\alpha_0=0\,, \tag{24}$$

so that the screening wave number is modified to

$$\kappa'=\kappa(1+\alpha_0)^{-1/2} \tag{25}$$

[κ being the inverse Debye length, defined by Eq. (22)].

In general, we must solve a transcendental equation for k. The screening length as determined by numerical solution of Eq. (23) as a function of density and field strength is given in Figs. 4 and 5.

The qualitative features of screening-length illustrations can be understood from elementary considerations. In the usual small-k approximation with few occupied levels the inverse screening length scales as

$$\kappa^2=\sum \kappa_s^{\,2}=\sum \omega_s^{\,2}/v_s^{\,2}\,, \tag{26}$$

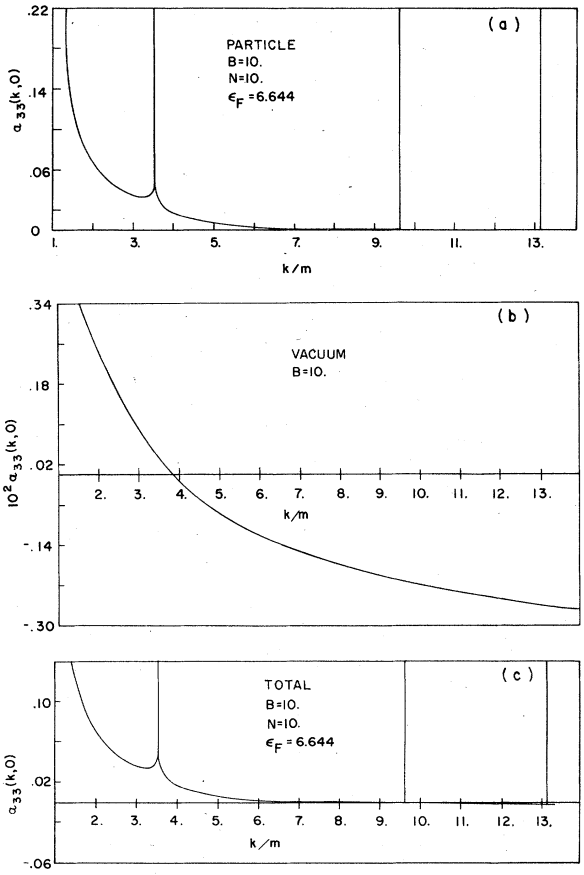

FIG. 3. $\alpha_{33}(k,0)$ versus k. Top level $s_F=2$ partially filled. $B=10B_*$, $n=10N_c$, $\epsilon_F=6.64m$. (a) Particle contribution. (b) Vacuum contribution. (c) Total a+b.

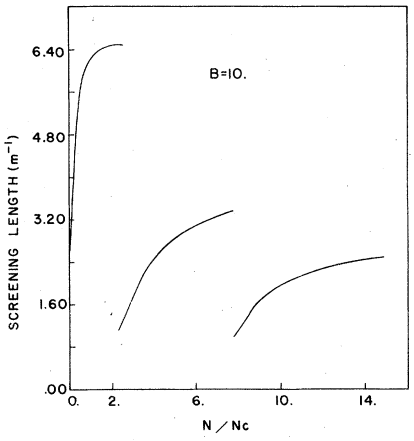

FIG. 4. Screening length in units of Compton wavelengths versus density for $B=10B_*$.

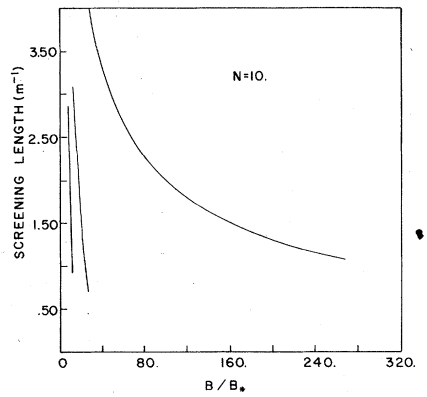

FIG. 5. Screening length versus B for $n=10N_c$.

where ω_s, the plasma frequency associated with level s, goes as

$$\omega_s \propto (n_s/\epsilon_F)^{1/2}, \tag{27}$$

where n_s is the number density, and with the Fermi velocity v_s being defined by

$$v_s = p_s/\epsilon_F. \tag{28}$$

Thus,

$$\kappa^2 \propto \sum \frac{n_s}{\epsilon_F} \frac{\epsilon_F^2}{p_s^2}. \tag{29}$$

Since κ_s^2 goes as $n_s/p_s^2 \propto 1/n_s$, the emptiest, i.e., the s_Fth, level contributes most to the sum. As B increases or n decreases, the top level empties, κ increases, and thus the screening length decreases. When the level is completely emptied, it disappears from the sum. Then κ decreases suddenly, and the screening length jumps to a new maximum.

The screening length obtained by solving the complete Eq. (23) is almost exactly that of the small-k limit up to the point where the Fermi level is almost empty. At that point the small-k expression, which is dominated by the s_Fth term, goes as $1/p_{s_F}$, becomes large, and the screening length goes to zero, whereas in the complete expression for $\alpha_{33}(k,0)$, the contribution of the s_Fth term goes to zero as p_{s_F} vanishes, and the screening length approaches a finite limit.

The scaling of successive maxima as a function of B can be understood from the following argument. For a given n, as B increases, the screening length decreases as a given level empties. However, at the beginning of each lower level the screening length jumps to a new maximum before decreasing. Since for completely filled shells all $p_s \propto B$, κ at the top of successively filled levels goes as

$$\kappa^2 = (\epsilon_F/B) \sum n_s/C_s, \tag{30}$$

where C_s are constants of order unity. For the case of only a few filled levels and $p_s \sim \epsilon_F \sim n/B$,

$$\kappa^2 \sim \epsilon_F n/B$$

$$\sim n^2/B^2, \tag{31}$$

so that the screening length scales as B/n.

Similarly for fixed B, as the number density increases and succeeding Landau levels are filled, the screening length for each level reaches a p-independent plateau; if $\epsilon_F \sim p_s$, $v_s \sim$ constant, and $\omega_e \sim n^{1/2}/p_s^{1/2} \sim 1/B^{1/2}$, the screening length goes as $B^{1/2}$, i.e., saturates.

Rigorously, the foregoing results apply only to the direction along the magnetic field, and thus their physical implications are limited. Horing's work[3] would imply that the Friedel-Kohn behavior coming from these results is highly anisotropic. For the nonrelativistic case in the strong-field limit, where only the lowest Landau level is occupied, Horing showed that off the parallel direction, the Friedel-Kohn shielding has an extremely fast exponential cutoff and is dominated by the strong-field counterpart of Debye-Thomas-Fermi shielding.

III. STATIC TRANSVERSE ELEMENT AND MAGNETIC POLARIZABILITY

The (differential) magnetic polarizability for arbitrary $\vec{k}$ was defined in Eq. (3). In the static case the magnetic polarizability $\vec{\xi}$ is related to the (differential) diamagnetic tensor $\vec{\nu}$ by

$$\vec{\xi}(\vec{k},0,B) = \vec{\nu}(\vec{k},0,B) - \vec{I}. \tag{32}$$

The relationship of $\vec{\xi}(0,0,B)$ to the quotient magnetic polarizability Ξ was given by Quinn.[5] To recapitulate, let us assume that to a system with a uniform magnetic field $\vec{B}_0$ and magnetization $\vec{M}_0$, we add a small perturbing field $\vec{B}_1$, generating a corresponding $\vec{M}_1$. Then

$$\vec{M}_0 = \Xi(B_0)\vec{B}_0, \tag{33a}$$

$$\vec{M}_1 = \vec{\xi}(B_0)\vec{B}_1, \tag{33b}$$

$$\vec{M}_0 + \vec{M}_1 = \Xi(|\vec{B}_0 + \vec{B}_1|)(\vec{B}_0 + \vec{B}_1), \tag{33c}$$

so that subtracting Eq. 33(a) from Eq. 33(c) and considering the limit as $\vec{B}_1$ tends to zero, we arrive at two separate cases. If $\vec{B}_1$ is perpendicular to $\vec{B}_0$ we obtain

$$\Xi(B_0) = M_1/B_1, \tag{34}$$

while for $\vec{B}_1$ parallel to $\vec{B}_0$ we get

$$\Xi(B_0) + B_0\Xi'(B_0) = M_1/B_1, \tag{35}$$

where $\Xi'(B_0)$ is the derivative of Ξ with respect to B_0. We can relate $\Xi(B_0)$ to $\vec{\xi}(B_0)$ in the $k \to 0$ limit by considering the polarization direction relative to $\vec{B}_0$. If $\vec{k}$ is perpendicular to $\vec{B}_0$, then taking $k = k\hat{x}$, $B_1 = B_1\hat{y}$,

$$\lim_{k_\perp \to 0} \xi_{22}(k_\perp, B_0) = \lim_{k_\parallel \to 0} \xi_{11}(k_\parallel, B_0)$$

$$= \lim_{k_\parallel \to 0} \xi_{22}(k_\parallel, B_0)$$

$$= \xi_\perp(B_0) = \Xi(B_0), \tag{36}$$

whereas

$$\lim_{k_\perp \to 0} \xi_{33}(k_\perp, B_0) = \xi_\parallel(B_0) = \Xi(B_0) + B_0\Xi'(B_0). \tag{37}$$

Thus for $\vec{k}$ parallel to $\vec{B}_0$ only the $\xi_\perp(B_0) = \Xi(B_0)$ is

accessible. The magnetic polarizability is now given by

$$\xi_{11}(k,0)=\xi_{22}(k,0)=\Pi_{11}(k,0)/k^2\,. \tag{38}$$

From Eq. (4) we find after a few transformations

$$\begin{aligned}\Pi_{11}(k,0)&=4\,\frac{e^3B}{2\pi}\sum_{s,\bar{s}}\int_{-\infty}^{\infty}dp\,\frac{n(\epsilon_{ps})(p^2+pk+m^2-\epsilon_{ps}{}^2)(\delta_{\bar{s},s-1}+\delta_{s,\bar{s}-1})}{\epsilon_{ps}(\epsilon_{p\bar{s}}{}^2-\epsilon_{ps}{}^2)}\\
&=\frac{e^3B}{2\pi}\Bigg\{\sum_{s=0}^{s_F}\ln\frac{p_s+\epsilon_F}{-p_s+\epsilon_F}+\sum_{s=0}^{s_F}\frac{1}{2}\,\frac{(2s+1)eB+k^2/2}{[(m^2+2seB)k^2+(k^2/2+eB)^2]^{1/2}}\Bigg[\ln\left|\frac{p_sk-(k^2/2+eB)}{p_sk+(k^2/2+eB)}\right|\\
&\qquad+\ln\frac{-(k^2/2+eB)p_s+(m^2+2seB)k+[(m^2+2seB)k^2+(k^2/2+eB)^2]^{1/2}\epsilon_F}{(k^2/2+eB)p_s+(m^2+2seB)k+[(m^2+2seB)k^2+(k^2/2+eB)^2]^{1/2}\epsilon_F}\Bigg]\\
&\qquad+\sum_{s=1}^{s_F}\frac{1}{2}\,\frac{(2s-1)eB+k^2/2}{[(m^2+2seB)k^2+(k^2/2-eB)^2]^{1/2}}\Bigg[\ln\left|\frac{p_sk-(k^2/2-eB)}{p_sk+(k^2/2-eB)}\right|\\
&\qquad+\ln\frac{-(k^2/2-eB)p_s+k(m^2+2seB)+[(m^2+2seB)k^2+(k^2/2-eB)^2]^{1/2}\epsilon_F}{(k^2/2-eB)p_s+k(m^2+2seB)+[(m^2+2seB)k^2+(k^2/2-eB)^2]^{1/2}\epsilon_F}\Bigg]\Bigg\}\end{aligned} \tag{39}$$

and Σ' indicates that the $(s=0)$ term is multiplied by $\frac{1}{2}$. In the nonrelativistic limit

$$\begin{aligned}\xi_{11}^{\rm NR}(k,0)=2\,\frac{e^3B}{2\pi}\,\frac{1}{k^2}\Bigg[&\sum_{s=0}^{s_F}{}'\frac{4p_s}{m}+\sum_{s=0}^{s_F}\frac{(2s+1)eB+k^2/2}{mk}\ln\left|\frac{p_sk-(k^2/2+eB)}{p_sk+(k^2/2-eB)}\right|\\
&+\sum_{s=1}^{s_F}\frac{(2s-1)eB+k^2/2}{mk}\ln\left|\frac{p_sk-k^2/2-eB}{p_sk+k^2/2-eB}\right|\Bigg].\end{aligned} \tag{40}$$

The static uniform $\Pi_{11}(0,0)$ vanishes. The finite $\xi_{11}(0,0,B)$ is determined from the first term in the k^2 expansion of $\Pi_{11}(0,0)$. The result is

$$\xi_{11}(0,0,B)=-4\,\frac{e^3B}{2\pi}\,\frac{1}{B^2}\sum_{s=0}^{s_F}{}'\left[p_s\epsilon_F-\frac{(m^2+4seB)}{2}\ln\frac{p_s+\epsilon_F}{-p_s+\epsilon_F}\right]. \tag{41}$$

In the nonrelativistic limit this becomes

$$\xi_{11}^{\rm NR}(0,0,B)=-4\,\frac{e^3B}{2}\,\frac{1}{mB^2}\sum_{s=0}^{s_F}{}'\,(\tfrac{2}{3}p_s{}^3-2seBp_s)\,, \tag{42}$$

which can also be derived as the $k\to 0$ limit of $\xi_{11}^{\rm NR}(k,0)$ given in Eq. (40).

A similar nonrelativistic expression was derived by Quinn, which, however, differs from Eq. (42) in that it refers to spinless particles. The distribution of particles over the Landau level and hence the p_s's are different for the spinless system. Formally, the spinless expression can be obtained by letting $2seB\to 2(s+\frac{1}{2})eB$ in $\xi_{11}^{\rm NR}(0,0,B)$.

Graphs of $\xi_\perp(0,0,B)$ as a function of B and density are given in Figs. 6 and 7. Both $\xi_\perp$ and $\xi_\perp^T$ (i.e., $\Xi_\perp$ and $\Xi_\perp^T$) are less than 0, reflecting the paramagnetic character of the system. (Quinn's spinless expression, of course, does not have this property.)

Since the long-wavelength limit is a k-independent function, there is no magnetic screening. However, the sharpness of the Fermi surface is manifested in the singularities in the magnetic polarizability. From Eq. (39) these singularities occur at

$$k=p_s+p_{s+1},\quad s=0,1,2,\ldots,s_F-1 \tag{43}$$

and also at the complex value

$$k=p_{s_F}+p_{s_F+1}\,. \tag{44}$$

(Note that p_{s_F+1} is pure imaginary.)

As the last level gets filled and the complex singularity approaches the real axis, the polarizability develops a finite minimum which becomes a singularity when the level is just filled. A graph of $\xi_{11}(k,0)$ is given in Fig. 8.

The character of the static magnetic polarizability as a function of k is dependent on the density and on the magnitude of $\vec{\mathrm{B}}$. At $k=0$, $\xi(k,0)$ is negative—the absolute magnitude increasing with density—and remains negative for all k. If only the lowest Landau level is partially occupied $\xi(k,0)$ has no infinities. As the density increases, $\xi(k,0)$ develops a minimum at $k=p_0$, referred to above. When the density for a given field strength is sufficiently high so that $\xi(k,0)$ can equal -1—

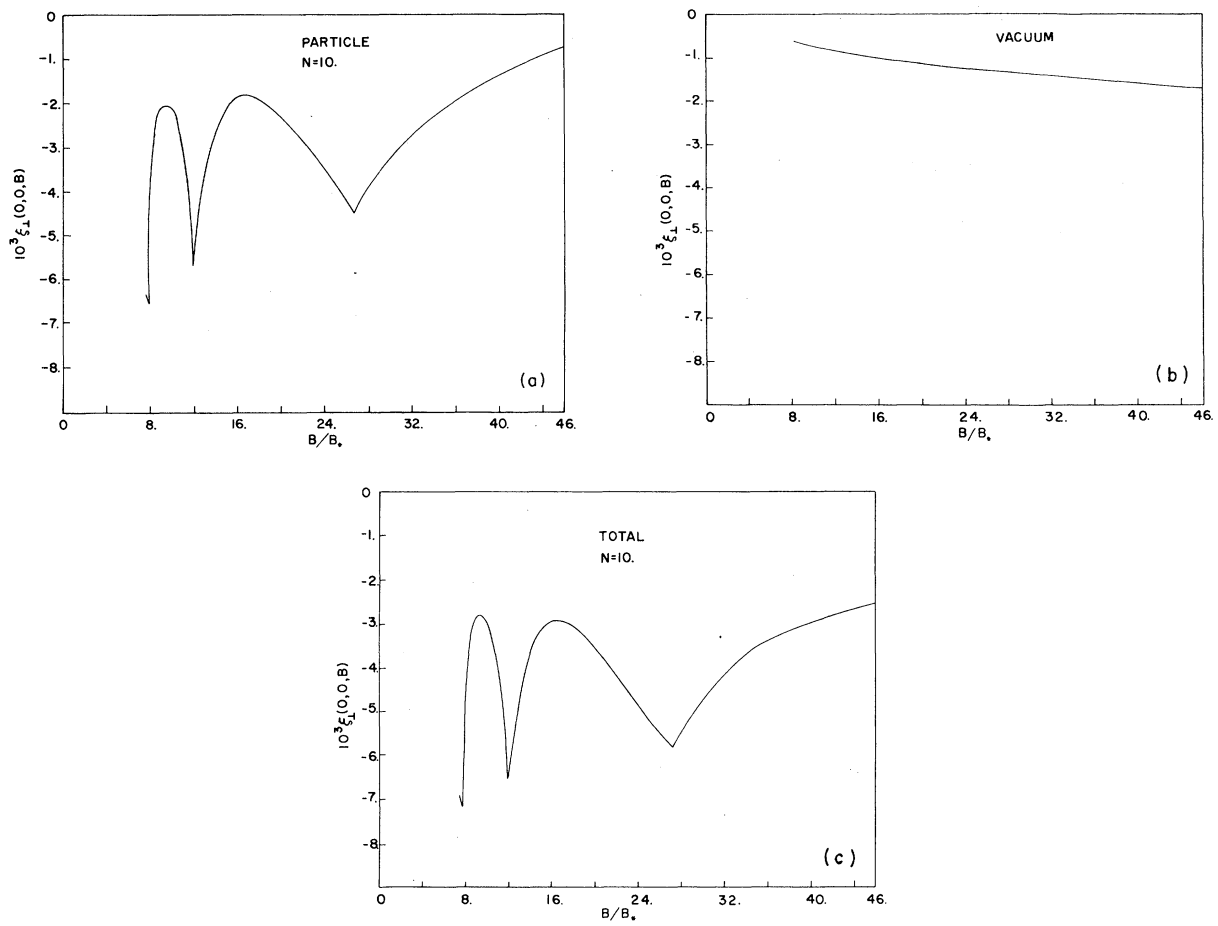

FIG. 6. Magnetic polarizability $\xi_{11}(0,0,B) \equiv \xi_\perp(0,0,B)$ versus B for $n = 10N_c$. (a) Particle contribution. (b) Vacuum contribution. (c) Total a+b.

a condition that obtains when the density equals or exceeds that of an almost-filled lowest level—the magnetic response function $\nu(k,0)$ vanishes. Since the induced magnetic intensity $B_1(k)$ is given by

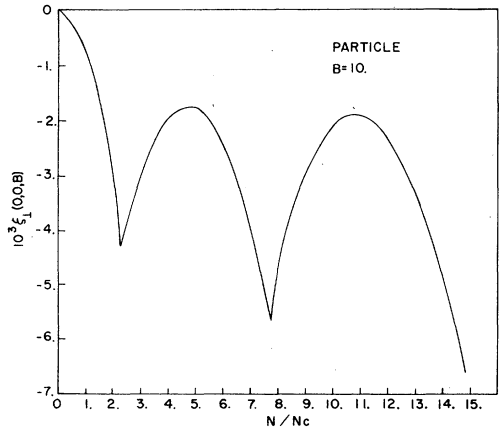

FIG. 7. $\xi_\perp(0,0,B)$ versus n for $B = 10B_*$ particle contribution. Vacuum contribution is constant -0.768×10^{-3}.

$B_1(k) = H_1(k)/\nu(k,0)$, the vanishing of $\nu(k,0)$ indicates a magnetic phase transition. In sum, with this model there exists for a given field strength a density above which there is a magnetic phase transition.

For real systems, small finite-temperature and collisional effects can strongly modify the character of $\xi_{11}(k,0)$ and can easily wash out the phase transition.

At finite temperatures the singularities are smoothed out and give rise to an oscillatory magnetic susceptibility. In a somewhat similar situation this oscillatory susceptibility was calculated by Lee and co-workers[15] for the nonrelativistic cases of $\vec{k}$ perpendicular to $\vec{B}$.

IV. DYNAMICAL LONGITUDINAL POLARIZABILITY AND THE PLASMA MODE

The dynamical ($\omega \neq 0$) $k = 0$ limit of the polarization matrix yields information on the normal modes of the plasma. In particular, the longitudinal element determines the plasma frequency of the sys-

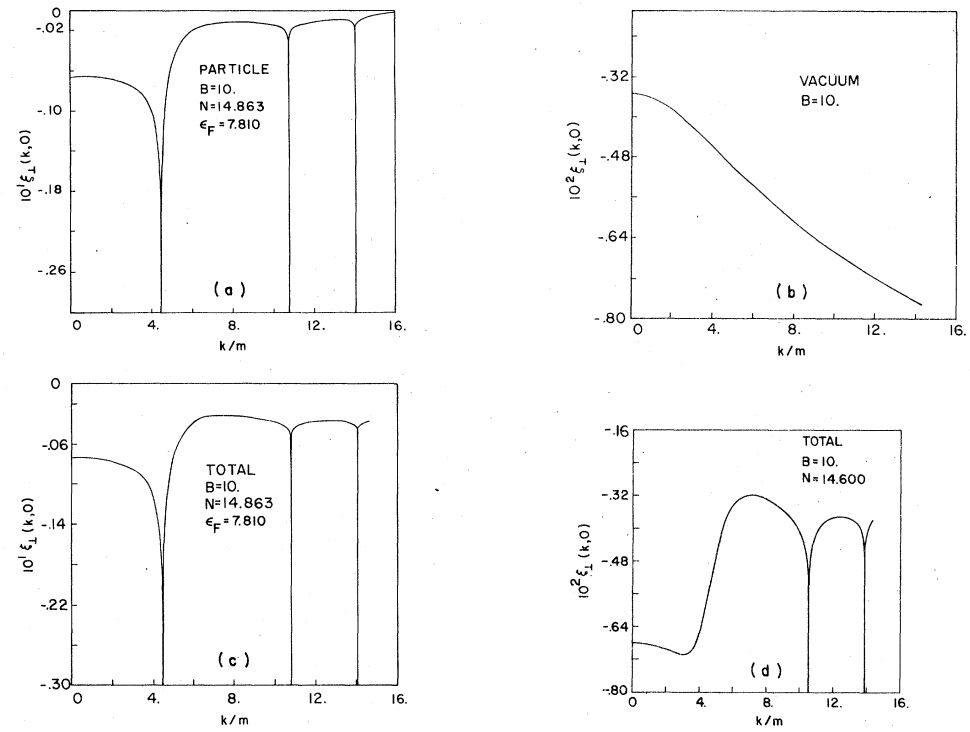

FIG. 8. $\xi_\perp(k,0)$ versus k for $B=10B_*, n=14.863\,N_c, \epsilon_F=7.810m$. Top level $s_F=2$ completely filled. Singularities are at p_2, p_1+p_2, and p_0+p_1. (a) Particle contribution. (b) Vacuum contribution. (c) Total a+b. (d) Comparative total for almost filled $s_F=2$ level.

tem.

The vacuum contribution to the longitudinal element of the polarization matrix $\Pi_{33}(0,\omega)$ was given in Eq. (36) of I. From Eq. (4) the particle contribution is

$$\Pi_{33}(0,\omega) = -\frac{e^3B}{2\pi}\int_{-\infty}^{\infty} dp \sum_{s,\bar{s}} \frac{n(\epsilon_{ps})}{\epsilon_{ps}}\left[\frac{-2p^2-\omega\epsilon_{ps}}{(\omega+\epsilon_{ps})^2-\epsilon_{p\bar{s}}^2}+\frac{-2p^2+\omega\epsilon_{ps}}{(\omega-\epsilon_{ps})^2-\epsilon_{p\bar{s}}^2}\right](\delta_{s\bar{s}}+\delta_{s-1,\bar{s}-1})$$

$$= 2\frac{e^3B}{2\pi}\sum_{s=0}^{s_F} a_s \int_{-p_s}^{p_s} \frac{(-2p^2-\omega\epsilon_{ps})\ (\omega^2-2\omega\epsilon_{ps})+(-2p^2+\omega\epsilon_{ps})\ (\omega^2+2\omega\epsilon_{ps})}{4\omega^2(p^2+m^2+2seB-\omega^2/4)}\frac{dp}{\epsilon_{ps}}$$

$$= 2\frac{e^3B}{2\pi}\sum_{s=0}^{s_F} a_s \int_{-p_s}^{p_s} \frac{m^2+2seB}{p^2+m^2+2seB-\omega^2/4}\frac{dp}{\epsilon_{ps}}$$

$$= 4\frac{e^3B}{2\pi}\sum_{s_\omega+1}^{s_F} a_s \frac{m^2+2seB}{(\omega/2)(m^2+2seB-\omega^2/4)^{1/2}}\tan^{-1}\frac{(\omega/2)p_s/\epsilon_F}{(m^2+2seB-\omega^2/4)^{1/2}}$$

$$+2\frac{e^3B}{2\pi}\sum_{s=0}^{s_\omega} a_s \frac{m^2+2seB}{(\omega/2)(\omega^2/4-m^2-2seB)^{1/2}}$$

$$\times\left\{\ln\left|\frac{(\omega/2)\epsilon_F+m^2+2seB-p_s[\omega^2/4-(m^2+2seB)]^{1/2}}{(\omega/2)\epsilon_F+m^2+2seB+p_s[\omega^2/4-(m^2+2seB)]^{1/2}}\right|\right.$$

$$\left.+\ln\left|\frac{p_s-[\omega^2/4-(m^2+2seB)]^{1/2}}{p_s+[\omega^2/4-(m^2+2seB)]^{1/2}}\right|\right\}, \tag{45}$$

with

$$a_s = 1, \quad s = 0$$
$$= 2, \quad s > 0, \tag{46}$$
$$s_\omega = -1 \text{ if } \omega < 2m$$
$$= \text{integer } [(\omega^2/4 - m^2)/2eB] \text{ if } \omega > 2m.$$

In the nonrelativistic limit this expression reduces to

$$\Pi_{33}^{NR}(0,\omega) = 4\frac{e^3 B}{2\pi}\sum_{s=0}^{s_F} a_s \frac{p_s}{m}, \tag{47}$$

which, in view of relation (14) relating p_s and the density, is the square of the usual plasma frequency. As ω goes to zero, $\Pi_{33}(0,\omega)$ goes to a positive constant, so that $\epsilon_{33}(0,\omega)$ goes to infinity as $-1/\omega^2$. As ω goes to infinity, $\Pi_{33}(0,\omega)$ goes as $-1/\omega^2$, so $\epsilon_{33}(0,\omega)$ approaches unity as $1/\omega^4$.

A plot of $\alpha_{33}(0,\omega)[= -\Pi_{33}(0,\omega)/\omega^2]$ is given in Fig. 9(a). The graph is characterized by $s_F + 1$ arctangent singularities at $\omega = 2(m^2 + 2seB)^{1/2}$, $s = 0, \ldots, s_F$, and a logarithmic singularity at $\omega = 2\epsilon_F$. From Eq. (36) of I the arctangent singularities are canceled by the corresponding singularities in the vacuum element. The logarithmic singularity coming at the boundary of the momentum integration (at the Fermi surface) is not canceled. The corresponding vacuum and total polarizations are displayed in Figs. 9(b) and 9(c).

For the general case the real solution to the equation

$$\epsilon_{33}(0,\omega) \equiv 1 + \alpha_{33}^T(0,\omega) = 0 \tag{48}$$

defines the plasma frequency ω_0 of the system. Graphs of the plasma frequency versus density and magnetic field strength are given in Figs. 10, 11, and 12. Some of the features of the plasma frequency curves can again be adduced from simple scaling arguments. The Landau-level structure is evident. For small enough B, the plasma frequency ω_0 goes as

$$\omega_0 \simeq \omega_p \equiv (4\pi n e^2/\epsilon_F)^{1/2} \tag{49}$$

as long as $\omega_p < 2\epsilon_F$.

For fixed and small B, $\epsilon_F \sim m$ and ω_0 roughly increases as $n^{1/2}$ as successive Landau levels are occupied. For fixed $B \gtrsim B_*$, and n becoming sufficiently large to fill the lowest level, the density dependence of ϵ_F comes into play and the increase of ω_p with n is slower than $\sqrt{n}$. In particular, for large, fixed B and n beginning to fill the lowest level,

$$\epsilon_F \sim p_0 \sim 2\pi^2 n/B, \tag{50}$$

and thus the plasma frequency

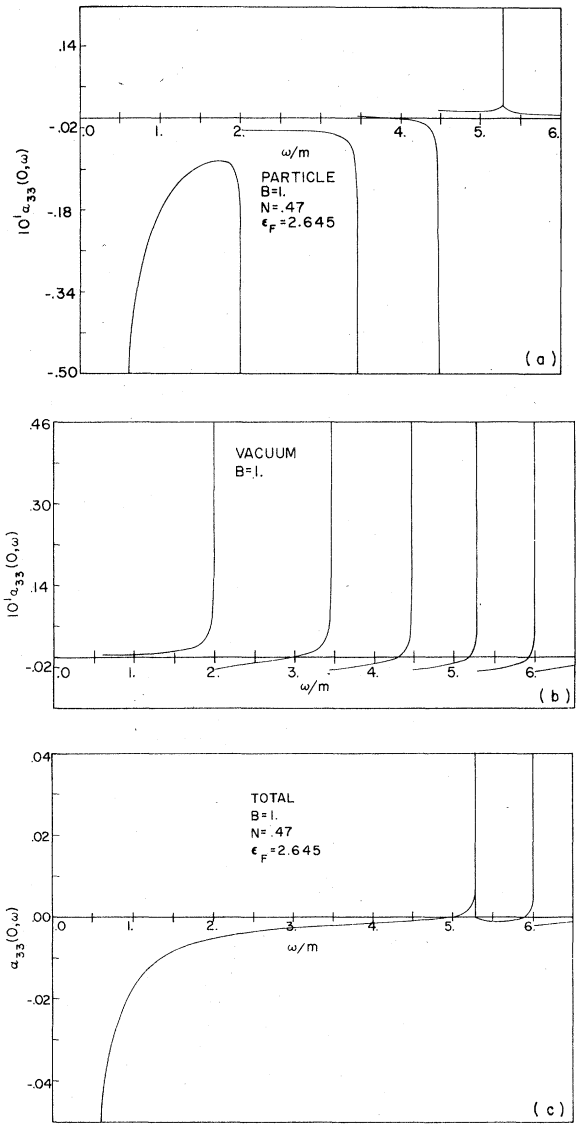

FIG. 9. $\alpha_{33}(0,\omega)$ versus ω for $B = B_*$, $n = 0.47N_c$, $\epsilon_F = 2.645m$. Top level $s_F = 2$ completely filled. (a) Particle contribution. (b) Vacuum contribution. (c) Total a+b.

$$\omega_0 \sim [4\pi n e^2/(2\pi^2 n/B)]^{1/2} = \left(\frac{2e^2}{\pi} B\right)^{1/2} \tag{51}$$

is independent of n; i.e., saturates. For this to happen the density has to be high enough for the plasma to be relativistic ($1 < n/N_c$), but low enough so that only the lowest level is occupied [$n/N_c < (B/B_*)^{3/2}$]: the two requirements are compatible for $B > B_*$ only, which is the condition for the plasma frequency saturation to occur. This process is illustrated in Fig. 10; for $B = B_*$ the slope of ω_0 merely decreases, whereas for $B = 100B_*$, ω_0 is almost flat over the range of densities n/n_c from 10 to 70.

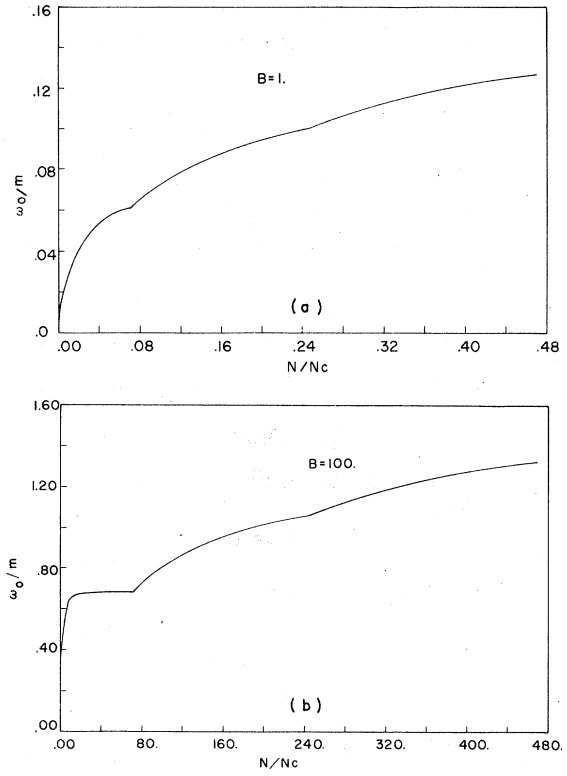

FIG. 10. Plasma frequency ω_0 versus n for (a) $B=B_*$ and (b) $B=100B_*$. Note the difference in the range of n.

For fixed density and increasing B the plasma frequency, as a level is being emptied, first increases and then decreases because of the oscillatory nature of the Fermi energy within that level—the longitudinal p_s decreasing while the transverse energy is increasing. In the lowest level the Fermi energy decreases with increasing B. The plasma frequency first rises reflecting its $\epsilon_F^{-1/2}$ dependence. For $n/N_c \lesssim 1$, and $B/B_* < 1/e^2$, the plasma frequency approaches its nonrelativistic limit $(4\pi ne^2/m)^{1/2}$. This behavior of the plasma frequency is shown in Fig. 11.

For large B the vacuum contribution qualitatively

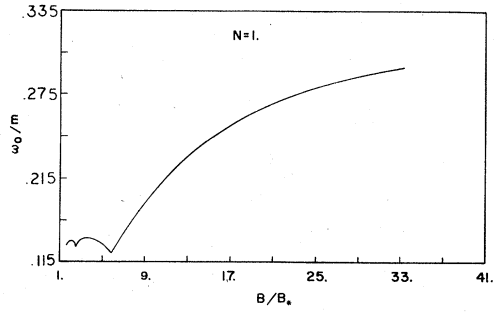

FIG. 11. ω_0 versus B for $n=N_c$. Lowest value of B corresponds to three filled levels.

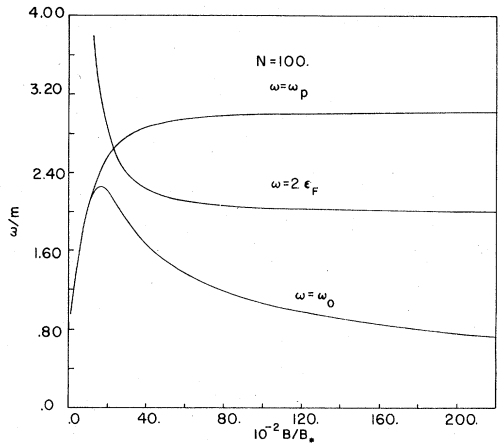

FIG. 12. Plasma frequency ω_0 versus B for $n=100N_c$ in the high-B $s_F=0$ domain. Graphs of $\omega=2\epsilon_F$ and $\omega=\omega_P$ $[=(4\pi ne^2/\epsilon_F)^{1/2}]$ are added for comparison.

affects the plasma frequency. Since the vacuum contribution to $\alpha_{33}(0,\omega)$ is positive for $\omega<2m$, the vacuum has the general effect of lowering the plasma frequency. For the case of $n/N_c \lesssim 1$ and $B/B_* > 1/e^2$, the plasma frequency decreases from its nonrelativistic plateau with increasing B.

For $n/N_c > 1$, the value of B such that only the lowest level is occupied is already substantial. Within the lowest level as B increases, the plasma frequency again first increases reflecting its $\epsilon_F^{-1/2}$ dependence. It peaks somewhat before the value of B for which

$$(4\pi ne^2/\epsilon_F)^{1/2} = 2\epsilon_F \tag{52}$$

and for increasing B monotonically decreases. This large-B behavior is illustrated in Fig. 12.

For a sufficiently large magnetic field ($>430\,B_*$) it was reported earlier[16] that the vacuum singularity structure gives rise to a longitudinal photon solution in which the vacuum $\alpha_{33}(0,\omega)=-1$ for ω between $2m$ and $2(m^2+2eB)^{1/2}$. The presence of particles modifies this photon solution to a double, that is a "two-plasmon," solution. The particle and total polarizability diverge to plus infinity on both sides of $\omega=2\epsilon_F$. If the particle number density is sufficiently low that $\epsilon_F < (m^2+2eB)^{1/2}$ and the field strength exceeds the photon threshold (so that the $2\epsilon_F$ particle singularity occurs between the $s=0$ and $s=1$ vacuum singularities, where the massive photon is only weakly damped), then the total polarizability will get pulled down from plus infinity through the value -1, giving the first plasmon solution. Before the point $2(m^2+2eB)^{1/2}$ the total polarizability, now dominated by the vacuum contribution, climbs through -1 again, giving rise to the second plasmon solution. Since the particle contribution is positive, the total po-

larizability will rise more rapidly than the vacuum part alone, and the second solution will be at a smaller value than the original photon solution. As the density increases, the two plasmon solutions will approach each other and finally merge. For larger densities no solutions of this type exist. A graph of the real part of the plasmon frequencies versus number density for a given B is presented in Fig. 13. In assessing the physical significance of this second resonance, it must be noted from Eq. (41) and Figs. 2 and 3 of I that the resonance is heavily damped near $\omega = 2m$.

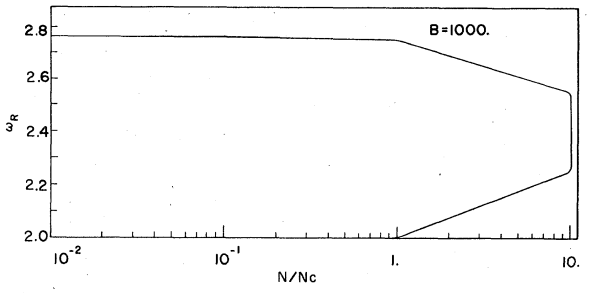

FIG. 13. Real double ("two-plasmon") solutions to $\epsilon_{33}(0,\omega)=0$ for $\omega > 2m$, $B > 437 B_*$. $B = 1000 B_*$. Smaller solution just greater than $2m$ until $n \simeq N_c$.

V. DYNAMICAL TRANSVERSE POLARIZABILITY AND TRANSVERSE MODE STRUCTURE

From Eq. (2) the normal modes of the system are determined by the dispersion relation

$$\text{Det}\,\left|\vec{\Delta}(\vec{k},\omega)+\vec{\Pi}^T(\vec{k},\omega)\right|=0\,. \tag{53}$$

For transverse polarization this reduces to

$$(\omega^2-k^2-\Pi_+^T)(\omega^2-k^2-\Pi_-^T)=0\,. \tag{54}$$

Thus for $k=0$ the previous equation becomes

$$\omega^2=\Pi_\pm^T(0,\omega)\,, \tag{55}$$

where

$$\Pi_\pm^T(0,\omega)=\Pi_{11}^T(0,\omega)\pm i\Pi_{12}^T(0,\omega)\,. \tag{56}$$

For parallel propagation the Kronecker delta factors for the $\Pi_\pm$ are

$$\Pi_\pm \to \delta_{s,\bar{s}\pm 1}\,. \tag{57}$$

Equation (4) in this case reduces to

$$\Pi_\pm(0,\omega)=-4\,\frac{e^3B}{2\pi}\sum_{s,\bar{s}}\delta_{s,\bar{s}\pm1}\int_{-\infty}^{\infty}dp\left[\frac{n(\epsilon_{ps})}{\epsilon_{ps}}\,\frac{\omega\epsilon_{ps}+2seB}{(\omega+\epsilon_{ps})^2-\epsilon_{\bar{p}\bar{s}}^{-2}}-\frac{n(\epsilon_{\bar{p}\bar{s}})}{\epsilon_{\bar{p}\bar{s}}}\,\frac{\omega\epsilon_{\bar{p}\bar{s}}-2\bar{s}eB}{(\omega-\epsilon_{\bar{p}\bar{s}})^2-\epsilon_{ps}^{\,2}}\right]. \tag{58}$$

After interchanging s and $\bar{s}$ in the second term, the matrix element becomes

$$\Pi_\pm(0,\omega)=-4\,\frac{e^3B}{2\pi}\sum_{s,\bar{s}}\delta_{s,\bar{s}\pm1}\int_{-p_s}^{p_s}\frac{dp}{\epsilon_{ps}}\left(\frac{\omega\epsilon_{ps}+2seB}{\omega^2+2\omega\epsilon_{ps}+2\,\Delta eB}-\frac{\omega\epsilon_{ps}-2seB}{\omega^2-2\omega\epsilon_{ps}-2\Delta eB}\right), \tag{59}$$

where $\Delta = s-\bar{s} = \pm 1$ corresponding to $\Pi_\pm$.

Since neither s nor $\bar{s}$ can be less than zero, s cannot equal zero in Π_+ and $\bar{s}$ cannot be zero in Π_-. Letting the following symbols indicate the thus-modified sums

$$\begin{aligned}
&\textstyle\sum'\text{: multiply by } \tfrac{1}{2} \text{ for } s=0\,,\\
&\textstyle\sum^+\text{: } s\neq 0 \text{ for } \Delta=1\,,\\
&\textstyle\sum^-\text{: } s\neq 0 \text{ for } \Delta=-1\,,
\end{aligned} \tag{60}$$

we get

$$\Pi_\pm(0,\omega)=4\,\frac{e^3B}{2\pi}\left[\sum_{s=0}^{s_F}{}'\ln\frac{\epsilon_F+p_s}{\epsilon_F+p_s}+\sum_{s=0}^{s_\omega^+}{}^+L_s^+(\omega)+\sum_{s=s_\omega^++1}^{s_F}{}^+T_s^+(\omega)+\sum_{s=0}^{s_\omega^-}{}^-L_s^-(\omega)+\sum_{s=s_\omega^-+1}^{s_F}{}^-T_s^-(\omega)\right], \tag{61}$$

where (note that s_ω^+ for Π_+ equals s_ω^- for Π_- and vice versa)

$$\begin{aligned}
s_\omega^\pm &= -1 \text{ if } \left|\omega^2\pm 2\Delta eB\right|/2\omega < m\\
&= \text{integer}\left[(\omega^2\pm 2\Delta eB)^2/4\omega^2-m^2\right]/2eB \le s_F \text{ if } \left|\omega^2\pm 2\Delta eB\right|/2\omega > m\,,
\end{aligned} \tag{62}$$

$$L_s^+(\omega)=\frac{1}{2}\,\frac{\omega^2-2(2s-\Delta)eB}{D_s^+(\omega)}\left[\ln\frac{D_s^+(\omega)+2\omega p_s}{D_s^+(\omega)-2\omega p_s}-\frac{\omega^2+2\Delta eB}{|\omega^2+2\Delta eB|}\ln\frac{D_s^+(\omega)\epsilon_F+|\omega^2+2\Delta eB|p_s}{D_s^+(\omega)\epsilon_F-|\omega^2+2\Delta eB|p_s}\right], \tag{63}$$

$$T_s^+(\omega)=-\frac{\omega^2-2(2s-\Delta)eB}{D_s^+(\omega)}\left[\tan^{-1}\frac{2\omega p_s}{D_s^+(\omega)}-\frac{\omega^2+2\Delta eB}{|\omega^2+2\Delta eB|}\tan^{-1}\frac{p_s|\omega^2+2\Delta eB|}{D_s^+(\omega)\epsilon_F}\right], \tag{64}$$

$$L_s^-(\omega)=-\frac{1}{2}\,\frac{\omega^2-2(2s+\Delta)eB}{D_s^-(\omega)}\left[\ln\frac{D_s^-(\omega)+2\omega p_s}{D_s^-(\omega)-2\omega p_s}+\frac{\omega^2-2\Delta eB}{|\omega^2-2\Delta eB|}\ln\frac{D_s^-(\omega)\epsilon_F+|\omega^2-2\Delta eB|p_s}{D_s^-(\omega)\epsilon_F-|\omega^2-2\Delta eB|p_s}\right], \tag{65}$$

$$T_s^-(\omega)=\frac{\omega^2-2(2s+\Delta)eB}{D_s^-(\omega)}\left[\tan^{-1}\frac{2\omega p_s}{D_s^-(\omega)}+\frac{\omega^2-2\Delta eB}{|\omega^2-2\Delta eB|}\tan^{-1}\frac{p_s|\omega^2-2\Delta eB|}{D_s^-(\omega)\epsilon_F}\right], \tag{66}$$

$$D_s^\pm(\omega)=\left[\,\left|\,(\omega^2\pm 2\Delta eB)^2-4\omega^2(m^2+2seB)\,\right|^{1/2}\right].$$

Graphs of $\alpha_\pm^T(0,\omega)$ $[=-\Pi_\pm^T(0,\omega)/\omega^2]$ are given in Figs. 14 and 15. It is convenient to divide the analysis of the expressions for $\Pi_\pm$ into a low-frequency regime where $\omega^2<2eB$ and a high-frequency region in which $\omega^2>2eB$. In the low-frequency domain, the total $\Pi_\pm$ is dominated by the particle contribution.

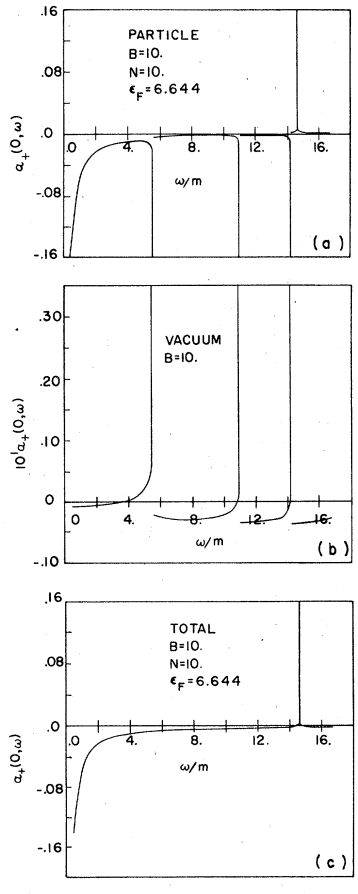

FIG. 14. $\alpha_+(0,\omega)$ versus ω for top level $s_F=2$ partially filled. $B=10B_*$, $n=10N_c$, $\epsilon_F=6.64m$. (a) Particle contribution. (b) Vacuum contribution. (c) Total a+b.

As ω goes to zero,

$$\lim_{\omega\to 0}\Pi_\pm(0,\omega)=16\,\frac{e^3B}{2\pi}\,\omega\Delta\sum_{s=0}^{s_F}\frac{p_s}{eB}, \tag{67}$$

so that $\Pi_\pm(0,\omega\to 0)$ is proportional to $\pm\omega$, $\alpha_\pm(0,\omega\to 0)$

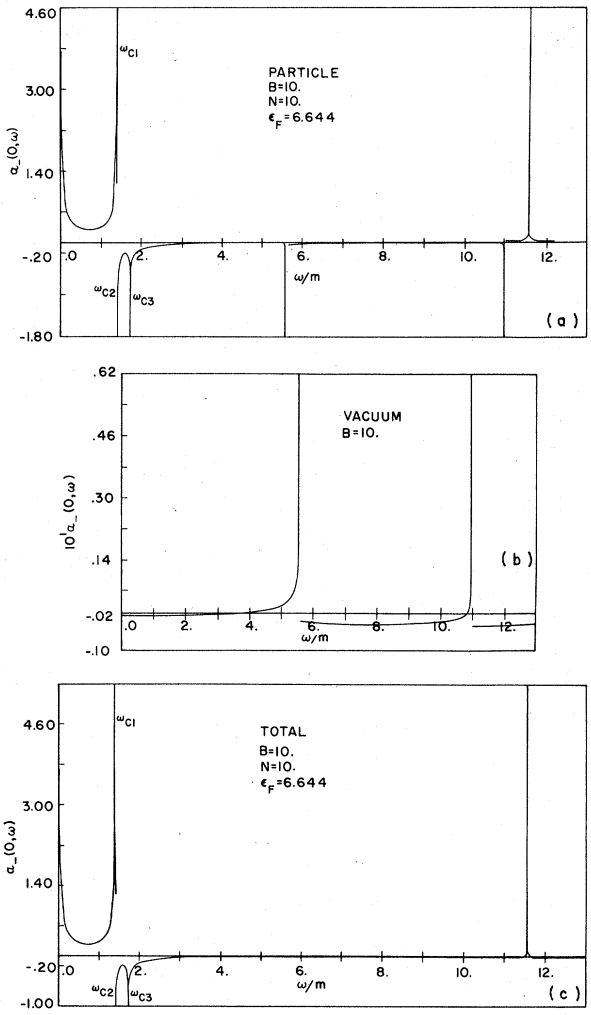

FIG. 15. $\alpha_-(0,\omega)$ versus ω for top level $s_F=2$ partially filled. $B=10B_*$, $n=10N_c$, $\epsilon_F=6.64m$. (a) Particle contribution. (b) Vacuum contribution. (c) Total a+b.

is proportional to $\mp 1/\omega$.

The structure of $\Pi_+(0,\omega\to 0)$ below $\omega^2<2eB$ is quite simple. The apparent logarithmic and arctangent infinities cancel one another term by term for each s within $T_s^{\pm}$ and $L_s^{\pm}$, so that Π_+ and α_+ do not exhibit any singularities and α_+ simply monotonically increases with increasing ω.

The structure of $\Pi_-(0,\omega)$ for $\omega^2<2eB$ is dominated by the presence of modified cyclotron modes. We will discuss the structure in terms of that of the related polarizability $\alpha_-(0,\omega)$, since this quantity can be more easily compared with the usual dispersion curve.

The qualitative features of $\alpha_-(0,\omega)$ as determined from the structure of Eq. (61) for $\Pi_-(0,\omega)$ are as follows: Each term $L_s^+(\omega)$ has a singularity at

$$\omega_{C1}=(\epsilon_F{}^2+2eB)^{1/2}-\epsilon_F \tag{68}$$

independent of s. A given term $L_s^+(\omega)$ switches to $T_s^+(\omega)$ at

$$\omega_{C2}^+(s)=[m^2+2(s+1)eB]^{1/2}-(m^2+2seB)^{1/2}. \tag{69}$$

The $L_s^+(\omega)$ term is finite at $\omega_{C2}^+(s)-0$. The $T_s^+(\omega)$ term has an inverse-square-root singularity at ω_{C2}^++0.

Similarly, each term in $L_s^-(\omega)$ has a singularity at

$$\omega_{C3}=\epsilon_F-(\epsilon_F{}^2-2eB)^{1/2} \tag{70}$$

independent of s. A given term $L_s^-(\omega)$ switches to $T_s^-(\omega)$ at

$$\omega_{C2}^-(s)=(m^2+2seB)^{1/2}-[m^2+2(s-1)eB]^{1/2}. \tag{71}$$

Again the $L_s^-(\omega)$ is finite at $\omega_{C2}^-(s)-0$, the $T_s^-(\omega)$ has a singularity at $\omega_{C2}^-(s)+0$.

However, $\omega_{C2}^+(s)=\omega_{C2}^-(s+1)$, so that the singularities associated with $T_s^{\pm}(\omega)$ cancel each other except at

$$\omega_{C2}^+(s_F)=[m^2+2(s_F+1)eB]^{1/2}-(m^2+2s_FeB)^{1/2}=\omega_{C2}. \tag{72}$$

It can be shown that

$$\omega_{C1}<\omega_{C2}\leq\omega_{C3}, \tag{73}$$

the equality obtaining in the case of a filled s_F level. Note that if $s_F=0$, $L_s^-(\omega)$ is absent from the sum so that there is no singularity at $\omega=\omega_{C3}$.

Thus the structure of $\alpha_-(0,\omega)$ for $\omega^2<2eB$ is as follows: $\alpha_-(0,\omega)$ decreases from plus infinity as ω increases from zero. It then increases, going to plus infinity as $\omega\to\omega_{C1}$. For $\omega>\omega_{C1}$ the polarization decreases to a finite limit as $\omega\to\omega_{C2}-0$. At $\omega=\omega_{C2}$, $\alpha_-(0,\omega)$ has an infinite discontinuity, rising from minus infinity at $\omega=\omega_{C2}+0$. It then decreases, becoming logarithmically infinite as $\omega\to\omega_{C3}$. It then increases from minus infinity as ω increases from ω_{C3}.

To determine the possible propagation of the relevant modes as a function of density and field strength, it is useful to analyze the relative amplitude of the resonances as a function of B and n. For a filled Fermi level, ω_{C2} and ω_{C3} coincide. For fixed B, as the density decreases, ω_{C3} increases, ω_{C2} is constant, and ω_{C1} begins to approach ω_{C2}. As the level is almost emptied, ω_{C1} and ω_{C2} almost coincide. When the level has just emptied, ω_{C2} jumps to the value of ω_{C3}. As a function of B for fixed density, the same relations between resonances occur as a level empties, only this time ω_{C2} also increases for increasing B. This variation of cyclotron resonance with B is illustrated in Fig. 16.

In the nonrelativistic limit

$$\omega_{C1}^{NR}=\omega_{C2}^{NR}=\omega_{C3}^{NR}=eB/m \tag{74}$$

and the structure of $\alpha_-(0,\omega)$ approaches that of the usual cyclotron mode. Detailed analysis of the modifications to the cyclotron mode will be presented in a subsequent publication.

In the large-B limit $eB\gg m^2$, $p_s{}^2$ we have

$$\omega_{C1}=\omega_{C2}=\omega_{C3}\sim(2eB)^{1/2}. \tag{75}$$

As was noted previously, if $s_F=0$, there is no

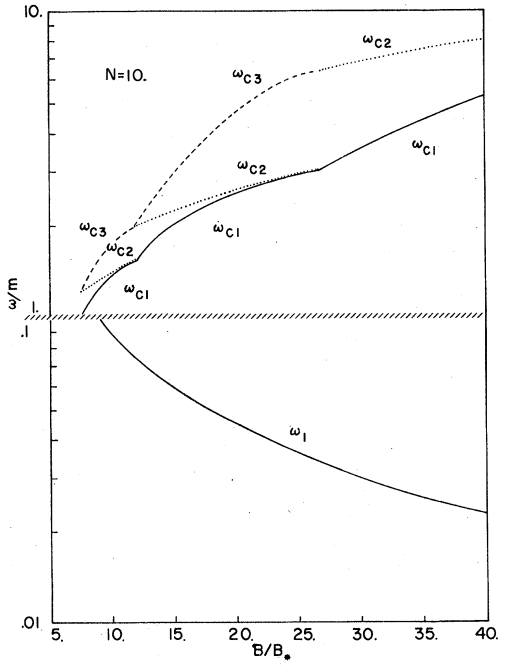

FIG. 16. Modified cyclotron resonances ω_{C1}, ω_{C2}, ω_{C3} versus B. ω_{C3} ceases to exist for $s_F=0$. Also, ω_1 versus B, where $\alpha_+(0,\omega_1)=-1$. The graph of ω_2 versus B [where ω_2 is the smallest solution to $\alpha_-(0,\omega_2)=-1$] would lie just above ω_{C3} (or above ω_{C2} for $s_F=0$) and is not separately displayed here.

resonance at ω_{C3}.

The resonance spacing in the nonrelativistic limit $m^2 \gg eB$, p_s^2 is

$$\omega_{C3} - \omega_{C1} \to (eB)^2/m^3.$$

In the large-B limit with $s_F = 0$,

$$\omega_{C2} - \omega_{C1} \to \tfrac{1}{2} p_0^2 \left(\frac{1}{m} - \frac{1}{(2eB)^{1/2}} \right) = \frac{2\pi^4 n^2}{B^2} \left(\frac{1}{m} - \frac{1}{(2eB)^{1/2}} \right). \tag{76}$$

When $\omega^2 > 2eB$, the cancellation of arctangent infinities between T_s^+ and T_{s+1}^- no longer occurs. However, the singularities of $T_s^{+\prime}$s for each s are canceled within each T_s^+. Both $\alpha_+(0,\omega)$ and $\alpha_-(0,\omega)$ have inverse-square-root singularities for each term in T_s^-. Namely, $\alpha_+(0,\omega)$ has negative infinities at

$$\omega = (m^2 + 2seB)^{1/2} + [m^2 + 2(s+1)eB]^{1/2}, \quad s = 0, 1, \ldots, s_F. \tag{77}$$

Similarly, $\alpha_-(0,\omega)$ has negative infinities at

$$\omega = (m^2 + 2seB)^{1/2} + [m^2 + 2(s-1)eB]^{1/2}, \quad s = 1, 2, \ldots, s_F. \tag{78}$$

However, from Eqs. (52) and (55) of I, these singularities are canceled by corresponding terms from the vacuum contribution $\alpha_{11}(0,\omega)$, so that the total polarizabilities are continuous and monotonic in the neighborhood of these values of ω.

For larger ω the polarizabilities enter the L_s domain. For each s with each L_s^+, the singularities again cancel. All L_s^- terms in $\alpha_+(0,\omega)$ have a positive logarithmic singularity at

$$\omega_+ = \epsilon_F + (\epsilon_F^2 + 2eB)^{1/2}. \tag{79}$$

Similarly, for the s_F terms in L_s^-, $\alpha_-(0,\omega)$ has a positive logarithmic singularity at

$$\omega_- = \epsilon_F + (\epsilon_F^2 - 2eB)^{1/2}. \tag{80}$$

If $s_F = 0$, $\alpha_-(0,\omega)$ has no singularity. This special feature of the resonance structure is again due to the absence of a $L^-(\omega)$ contribution if $s_F = 0$.

After this singularity, the particle contribution to $\alpha_\pm^T(0,\omega)$ goes to zero as $1/\omega^4$, while the total polarizabilities are dominated by the vacuum contribution which includes infinities at

$$\omega = (m^2 + 2seB)^{1/2} + [m^2 + 2(s \pm 1)eB]^{1/2}, \quad s = s_F + 1, \; s_F + 2, \ldots. \tag{81}$$

To return to a discussion of mode structure, the mode described by $\alpha_+(0,\omega)$ is generally referred to as the left-hand circularly polarized wave. The wave propagates for $\omega > \omega_1$, where $\alpha_+(0,\omega_1) = -1$. Below this cutoff, the index of refraction $[1 + \alpha_+(0,\omega)]^{1/2}$ is imaginary. For field strengths and densities of interest here, the plasma frequency ω_p is less than the classical cyclotron frequency ω_c ($\equiv eB/\epsilon_F$). The cutoff is larger than but of the order of classical cutoff for $\omega_C > \omega_p$, i.e., $\omega_1 \gtrsim \omega_p^2/\omega_C$. This cutoff is well below any of the resonances discussed above and approaches zero as B increases or n decreases.

The mode described by $\alpha_-(0,\omega)$ for $< \omega_{C^*}$ (where ω_{C^*} is somewhere between ω_{C1} and ω_{C3}) is the electron wave, or whistler. The propagation region for this right-hand circularly polarized wave for higher frequencies is complicated by the existence of two negative resonances. When ω_{C2} coincides with ω_{C3}, as is the case with an almost full Fermi level, the cutoff ω_2 for the mode lies just above ω_{C3} and the wave can propagate for $\omega > \omega_2$ [where ω_2 is the highest frequency for which $\alpha_-(0,\omega_2) = -1$]. For ω_{C2} and ω_{C3} more widely spaced, there is generally a propagation region in the interval ω_{C2} to ω_{C3}. The excluded region surrounding the logarithmic resonance at ω_{C3} tends to be quite narrow.

VI. SUMMARY

In this paper we have explicitly calculated the elements of the particle contribution to the polarization matrix for a relativistically dense plasma in an arbitrarily strong external magnetic field for the case of $\vec{k} \parallel \vec{B}$. Upon combining these results with the corresponding vacuum elements displayed in I, we were able to analyze the corresponding static electric and magnetic properties and normal modes of the physical system. The new physical features that have emerged from this analysis can be attributed to three main sources: the ultrastrong value of the magnetic field ($B > B_* = m^2/e$), the relativistic Fermi energy ($n > N_c = m^3$) of the electrons, and the small number of Landau levels occupied; some additional new features were shown to come into existence for $n \gtrsim N_c/e^2$ and $B \gtrsim B_*/e^2$.

The new effects can be briefly summarized as follows. (1) The fact that only a few Landau levels are occupied brings into focus the sharp dependence of the screening length κ^{-1} on the population of the individual levels. Since each level contributes to the screening length in the proportion of n_s/v_s^2, and since $v_s \sim n_s$, paradoxically the emptiest level dominates, enhancing the screening properties of the plasma with increasing B within each level. In particular, for the case of an ultrastrong magnetic field where only the 0 level is occupied, $\kappa^{-1}(B)/\kappa^{-1}(B=0)$ for a given density is of

the order $(n/N_c)B_*/B$, raising the interesting possibility of the formation of a strongly coupled one-dimensional plasma. (2) The relativistic particle energies make it impossible to separate the spin and orbital contribution to the static magnetic polarizability $\xi_\perp(0,0;B)$, which now exhibits the resulting paramagnetic behavior, together with the expected oscillatory character. When only the 0 level is occupied the rapidly decreasing $(\sim B^{-3})$ value of the particle contribution renders the vacuum contribution (which is a slowly increasing function of B) competitive even for high values of the density. For finite k the singularities of $\xi_\perp(k,0;B)$ point to the possibility of a magnetic phase transition known from nonrelativistic analyses; but in the case of only the 0 level being occupied, the condition for the phase transition is met only when the density exceeds a critical value. (3) The plasma frequency ω_p develops a remarkable magnetic field dependence whose origin lies in the combination of all the physical effects listed above. The relativistic Fermi energy is responsible for the reduction of the plasma frequency below its nonrelativistic value and for its oscillatory behavior with increasing B in the wake of the oscillating Fermi energy. Once, however, only the 0 level is occupied, for ultrastrong B values the nonrelativistic value of the plasma frequency is quickly restored, except for densities high enough to result in ω_p exceeding $2m$ $[n \simeq (1/4\pi e^2)N_c]$; the pair-creation resonance of the polarizability at $\omega = 2\epsilon_F$ prevents the plasma frequency from exceeding this limit, resulting in it passing through a maximum for some value of the magnetic field. (4) The vacuum-supported longitudinal photon, whose existence itself is a consequence of the ultrastrong magnetic field $[B \simeq (\pi/e^2)B_*]$,[16] splits into two longitudinal modes, one in the vicinity of $2\epsilon_F$, the other somewhat below the frequency of the vacuum longitudinal photon. Both of these longitudinal modes disappear, and the longitudinal photon is suppressed as the density exceeds a critical limit. (5) The relativistic structure of the one-particle energies leads to a very peculiar splitting of the nonrelativistic cyclotron resonance. The width of the satellite region itself widens with increasing B, undergoing discontinuous structural changes at each value of B when a level empties.

Although we have derived the full k and ω-dependent polarizabilities, we have analyzed in detail only the $\omega = 0$ and $k = 0$ limits. By doing so we neglected two related features of the full $(k_\parallel, \omega)$ system: first, the expected singularities at the Fermi surface $\omega = \vec{k}\cdot\vec{p}/\epsilon_F$ together with their contribution to the imaginary part resulting from these singularities, second, the difference between the structure of the value of $\epsilon(k,\omega)$ in the vicinity of the mass-shell $\omega \approx k$ and its "hydrodynamic" value $\epsilon(k,0)$. From the point of view of the propagation of those transverse modes whose phase velocities are of the order of, or greater than, c, the difference might be significant.

In future papers we will analyze the cyclotron mode in more detail, extend our considerations to the full $(k_\parallel, \omega)$ case, and consider the case where $\vec{k} \perp \vec{B}$.

[1] M. J. Stephen, Phys. Rev. 129, 997 (1962).
[2] N. J. Horing, Ann. Phys. (N.Y.) 31, 1 (1965).
[3] N. J. Horing, Phys. Rev. 186, 434 (1969).
[4] J. J. Quinn and S. Rodriquez, Phys. Rev. 128, 2487 (1962).
[5] J. J. Quinn, J. Chem. Solids 24, 933 (1963).
[6] M. P. Green, H. J. Lee, J. J. Quinn, and S. Rodriquez, Phys. Rev. 177, 1019 (1969).
[7] V. Canuto and H. Y. Chiu, Phys. Rev. 173, 1210 (1968).
[8] V. Canuto and J. Ventura, Astrophys. Space Sci. 18, 104 (1972).
[9] J. J. Quinn, Phys. Rev. Lett. 16, 731 (1966).
[10] H. J. Lee, V. Canuto, H. Y. Chiu, and C. Chiuderi, Phys. Rev. Lett. 23, 390 (1969).
[11] V. N. Tsytovich, Zh. Eksp. Teor. Fiz. 40, 1775 (1961) [Sov. Phys.—JETP 13, 1249 (1961)].
[12] G. Kalman, Bull. Am. Phys. Soc. 12, 777 (1967); B. Prasad and G. Kalman, *ibid.* 13, 309 (1968); G. Kalman and B. Prasad, Bull. Am. Astron. Soc. 1, 195 (1969).
[13] P. Bakshi, R. A. Cover, and G. Kalman, Phys. Rev. D 14, 2532 (1976).
[14] M. H. Johnson and B. A. Lippmann, Phys. Rev. 76, 828 (1949); 77, 702 (1950).
[15] H. J. Lee, M. P. Green, and J. J. Quinn, Phys. Rev. Lett. 19, 428 (1967).
[16] R. A. Cover and G. Kalman, Phys. Rev. Lett. 33, 1113 (1974).